

Wear-resistant and anticorrosion mechanism for transmission friction pairs in marine environment

Ke Ning¹, Qi Wang¹, Jianmei Wang^{1,2,✉}, Wengang Ning³

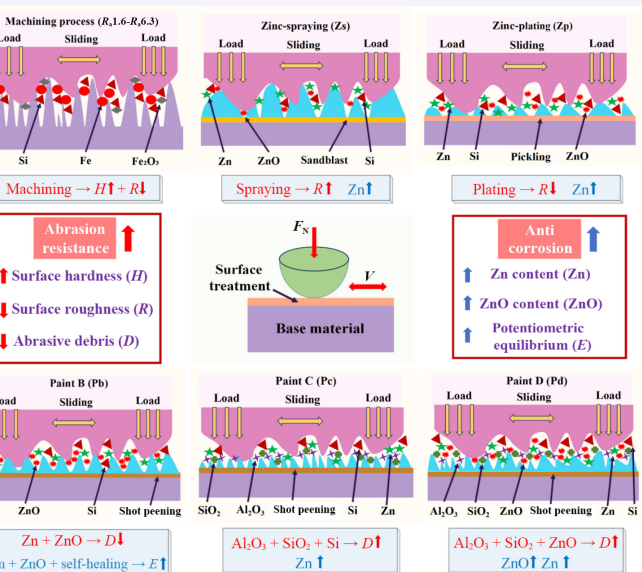
Cite this article: Ning K, Wang Q, Wang JM, et al. *Friction* 2025, **13**: 9441037. <https://doi.org/10.26599/FRICT.2025.9441037>

ABSTRACT: Friction pair coatings are highly susceptible to failure in corrosive marine environments. To enhance their service performance, this study focuses on the friction pairs in the main shaft transmission of offshore wind turbines and investigates the wear and corrosion resistance of different surface treatment processes. A wear theory model is developed on the basis of dynamic changes in the contact area to predict wear under dry friction and corrosive conditions. The results indicate that the Interzinc B coating results in the best overall performance in terms of friction, wear, and corrosion resistance. Rough and high-hardness surfaces increase the friction coefficient, whereas Zn powder and ZnO adhesive not only produce less abrasive debris but also form a micro/nanoparticle self-lubricating mechanism, reducing surface wear. Compared with the traditional zinc spraying process, the friction coefficient can be increased by 28.4%, whereas the wear amount can be reduced by 76.2%. The release of Zn^{2+} and the oxidation reaction mechanism enhanced the self-healing ability of the passive film, improving its anticorrosion ability. The maximum error between the finite element analysis of coating wear and the test results is only 6.26%, which verifies the accuracy of the wear theory model and provides guidance for the precise design of wind turbine transmission friction pairs.

KEYWORDS: wear; corrosive; wear prediction; surface treatment process; coating; wind turbine

1 Introduction

Given the extreme conditions of high salt spray, high humidity, and corrosive environments in marine environments, the application of wear-resistant and anticorrosion coatings is one of the main measures used to prevent the failure of transmission friction pairs [1–3]. This study focuses on the transmission connection friction pairs of offshore wind turbines. With the growing global demand for clean energy, offshore wind power has played an increasingly important role as a sustainable energy solution [4]. Figure 1 shows the structural diagram of the main shaft transmission friction pair of a specific model of a wind turbine. The main shaft transmits torque through friction interfaces (threaded connection surfaces) with the coatings of the hub and gearbox. The coatings on these friction interfaces provide wear resistance and corrosion protection to withstand the highly



corrosive conditions of the marine environment [5]. Therefore, excellent wear and corrosion resistance are necessary while meeting the required friction forces on the friction pairs. Research on friction-wear and wear prediction for surface coatings of transmission connection friction pairs of offshore wind turbines is crucial [6].

The main types of surface coatings for transmission connection friction pairs in offshore wind turbines include zinc coatings (zinc-spraying, zinc-plating) and paint-spraying (epoxy zinc-rich paint) [7]. Many scholars have explored the wear resistance and anticorrosion behavior of surface coatings on key components of wind turbines. Lee [8] investigated the effects of substrate surface roughness on the corrosion and wear-corrosion resistance properties of electroless Ni–P (ENP) coatings on glass fiber-reinforced plastic (GFRP) composites in wind turbine blades through wear and corrosion tests. The results show that

¹ Engineering Research Center Heavy Machinery Ministry of Education, Taiyuan University of Science and Technology, Taiyuan 030024, China. ² Shanxi Institute of Engineering Technology, Yangquan 045000, China. ³ Technology Center, Taiyuan Heavy Machinery Group Co., Ltd., Taiyuan 030024, China.

✉ Corresponding author. E-mail: wjmhdb@163.com

Received: August 15, 2024; Revised: October 10, 2024; Accepted: November 4, 2024

© The Author(s) 2025. This is an open access article under the terms of the Creative Commons Attribution 4.0 International License (CC BY 4.0, <http://creativecommons.org/licenses/by/4.0/>).

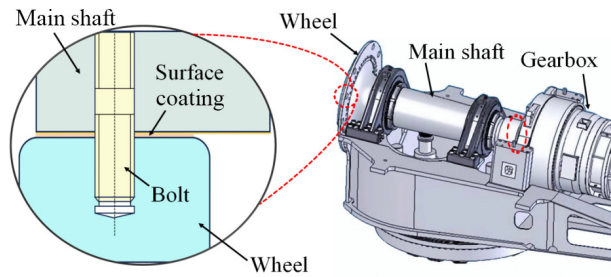


Fig. 1 Transmission connection friction pairs for main shaft of a certain model wind turbine.

improving the surface roughness of the substrate can improve the corrosion and wear resistance of ENP coatings. Wei et al. [9] revealed the influence of tungsten carbide (WC) on the microstructure and wear resistance of iron-based coatings prepared by laser cladding on the surface of wind power gears, and the results revealed that increasing the WC content can improve the wear resistance of laser-fused cladding. In a study of wear-resistant and anticorrosion zinc coatings on steel surfaces, Souza et al. [10] conducted friction and wear tests on thermally sprayed zinc coatings and Zn-Fe electrodeposited coatings in a 3% NaCl solution. These findings suggested that the wear-corrosion resistance of the zinc-sprayed coatings was superior to that of the Zn-Fe electrodeposited coatings. Pinger et al. [11] investigated the wear behavior of zinc-plated coatings by varying the friction roll, load, and total number of cycles during the wear process. Their results demonstrated the effective wear resistance of zinc-plated coatings containing a hard intermetallic Zn-Fe compound phase and an external pure Zn phase. Liu et al. [12] analyzed the influence of environmental factors on the anticorrosion performance of thermally sprayed zinc coatings through salt spray and electrochemical corrosion tests. The results showed that the corrosion protection of zinc-sprayed coatings is limited in extreme environments and under conditions of increased pollution. Therefore, in anticorrosion coating systems designed for metal cathodic protection, epoxy zinc-rich paint has gradually become a widely used and effective anticorrosion coating [13]. To research the wear resistance and anticorrosion properties of epoxy zinc-rich coatings on metal surfaces, Gerengi et al. [14] compared and analyzed the corrosion characteristics of epoxy zinc-free and zinc-rich coatings in a 5% NaCl solution. They concluded that epoxy zinc-rich coatings have superior anticorrosion properties. Lin et al. [15] studied the anti-wear properties of coatings under the synergistic effect of shot peening and zinc-rich epoxy coatings. Shot peening provided mechanical support, whereas the epoxy coating acted as a cushion against friction, thereby enhancing the wear resistance of the coating as a whole. In addition to other studies on the behavior of wear-resistant and anticorrosive coatings, Özkan et al. [16] investigated the wear and corrosion resistance of graphene oxide coatings via tests, and the results demonstrated that the graphene oxide coatings exhibited excellent anticorrosion properties in extremely corrosive media, reacted with zinc dialkyl dithiophosphates (ZDDPs), and formed a friction film, which provided additional wear resistance. Wu et al. [17] concluded that CoCrFeNi HEA/WC composite coatings (HEACC) have greater wear and corrosion resistance than H13 steel substrates do by investigating the phase transformation, organizational evolution, and wear corrosion resistance of the coatings. However, there is a lack of systematic research on wear-resistant and anticorrosion coatings for the transmission connection friction pairs of offshore wind turbines.

In research on the theory of wear prediction for friction pair surfaces, Velten et al. [18] proposed a wear prediction method

based on artificial neural networks as early as 2000. Although this method calculates the amount of wear with a significant error when a large number of randomly selected test datasets are considered, even relatively uncertain predictions contribute to advancements in tribology. In 2004, Hsu and Shen [19] developed multiple wear models to predict the wear of ceramics, achieving a model accuracy within ± 1 order of magnitude. Later, Abdelgaied et al. [20] established a wear prediction model for artificial knee joints on the basis of new wear patterns and formulas. While this computational model has been widely utilized for wear prediction and optimization of artificial knee joint designs, it does not apply to other polymer materials and lacks generalizability. Liu et al. [21] proposed a numerical calculation method for railway wheel wear that combines Archard's equation with spatial statistical methods, providing a more realistic prediction of wear than traditional methods do. Friction and wear models have been greatly developed and improved during the grinding process. Zhang et al. [22–24] proposed a novel model that accurately predicts the maximum undeformed chip thickness in grinding processes. Moreover, a new single-grit grinding/scratching method was developed, with speeds increasing by 4–7 orders of magnitude. Finally, breakthroughs in grinding theory have promoted the development of new grinding methods, significantly improving the efficiency and effectiveness of traditional grinding processes. With the continuous advancement of wear theory research and innovations in finite element technology, Cao et al. [25] established a physical model for wear prediction in grinding machines on the basis of the finite element method and numerical simulation. This model enables numerical prediction and trend analysis of the grinding temperature, surface morphology, and amount of wear, achieving a relative error of 9.84% between the theoretical and actual wear values. Wang et al. [26] developed a wear prediction model for U-rings by studying their wear characteristics in strong wind environments. The simulation results for the wear depth are closely aligned with the test values, with an error of only 1.56%. Necpal and Vozár [27] utilized DEFORM software in conjunction with a wear model to predict tool wear during lathe machining, optimizing the cutting parameters and improving tool life. Currently, methods for predicting wear in wear-resistant and anticorrosion coatings for transmission connection friction pairs in offshore wind turbines remain unclear.

Taking the transmission connection friction pairs for the main shaft of offshore wind turbines as the research object, this study investigates the wear resistance and anticorrosion behavior of the machining and coating process of the friction pair surface, especially analyzing the friction coefficient, wear pattern, wear amount, and electrochemical characteristics of the corrosive medium in detail, as well as the preferred coating on the surface of the friction pairs on the basis of the wear mechanisms of various coatings. To predict coating wear under dry and corrosive friction conditions, a theoretical model of ball-disc wear is proposed, in which the change in the real contact area during the wear process leads to a change in the contact area. In addition, the wear amount of different coating processes are dynamically simulated via the Fortran language for finite element secondary development, which is proposed to provide theoretical guidance and a technical reference for the coating design of wind turbines.

2 Materials preparation and testing methods

2.1 Materials preparation and coating process

Taking the transmission connection friction pairs of offshore wind

turbine main shafts as the study objects and using 34CrNiMo6 as the base material, the samples were all obtained by cutting them from a solid main shaft, and the size was 20 mm × 10 mm × 3 mm. The sample was processed according to the surface treatment process of the friction pairs of the main shafts of the wind turbine. Figure 2 shows the process flow chart of surface treatment for friction pairs.

R_a 1.6–6.3 are determined on the basis of the general machining requirements for wind turbine transmission friction pairs. Before coating, the metal surface is thoroughly cleaned to remove dirt, grease, rust, and other impurities [28]. Sandblasting is needed, and the surface should achieve a S_a 2.5 grade (ISO 8501) with a roughness of $R_y = 60\text{--}100\ \mu\text{m}$ before zinc spraying (Zs). Pickling must be performed prior to zinc plating (Zp) to remove oxides and other surface contaminants, thereby improving the adhesion of the coating. The zinc spraying process was conducted with an air pressure of 0.5–0.6 MPa, a spray angle of 75°–80°, and a spray distance of 100–120 mm. Zinc plating involves immersing the sample in a zinc-acid salt solution to achieve zinc adhesion through electroplating. The coating thickness for zinc spraying exceeds 100 μm , whereas the thickness for zinc plating is greater than 20 μm . Three types of epoxy zinc-rich coatings—Interzinc B,

Hempel C, and Interzinc D—were selected for surface paint spraying, referred to as Pb, Pc, and Pd, respectively. Before paint spraying, the surface must undergo shot peening, achieving a S_a 2.5 grade (ISO 8501). The film thickness of Pb and Pc after spraying should reach 75–100 μm , whereas the film thickness of Pd should be greater than 50 μm but not exceed 100 μm . The macroscopic and microscopic diagrams of the different surface treatment processes are shown in Fig. 3.

2.2 Characterization

The surface profile and roughness were measured via a surface roughness tester (SJ-420, Mitutoyo, Japan), which has a measurement accuracy of 0.001 μm . Three measurements were taken for each sample to obtain the average value. The surface hardness was tested via a Vickers hardness tester (MHVS-10V, Shanghai Aolong, China), with each sample measured five times, and the average value was recorded. The test results are shown in Fig. 4, HV is the unit of Vickers hardness. Compared with those of the machining process, the hardness values of the zinc coating (zinc spraying and zinc plating) and paint-spraying processes increased by 1.44% and 9.54%, respectively. This increase is primarily because the zinc coatings underwent surface

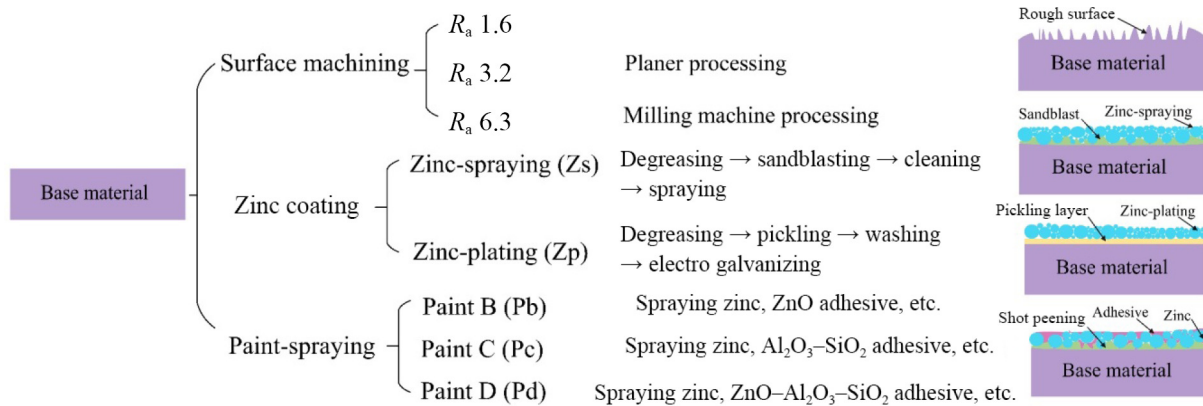


Fig. 2 Surface treatment process flow chart of friction pairs.

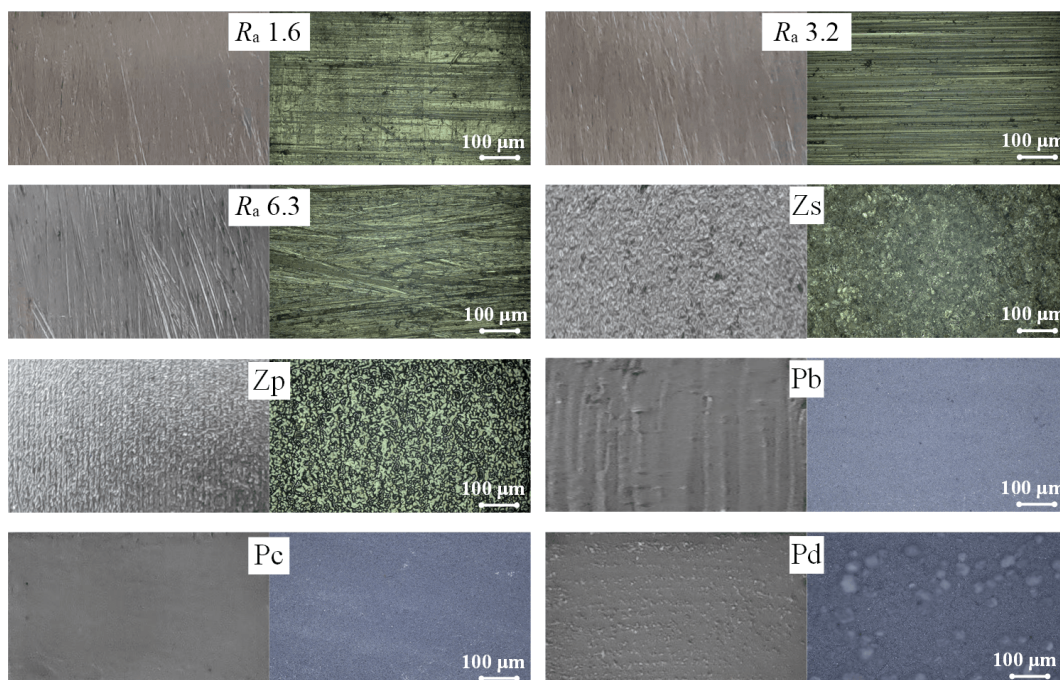


Fig. 3 Macro- and micrographs of different surface treatment processes.

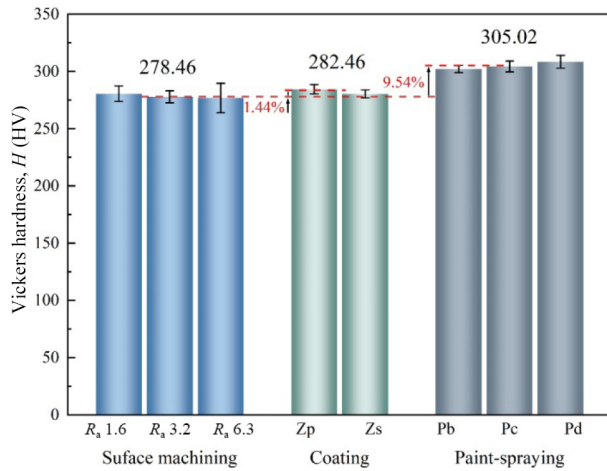


Fig. 4 Hardness of different surface treatment processes.

sandblasting, whereas the paint-spraying process involved surface shot blasting. Both sand blasting and shot blasting are forms of surface cold work hardening. Cold work hardening generates significant internal stress and plastic deformation on the surface of metal materials, leading to an increase in surface hardness [15].

After the friction-wear test was complete, the samples were left in their original state to observe the morphology of the abrasive debris and corrosive substances. The samples were then ultrasonically cleaned using an alcohol solution. Once dried, the surface and wear morphology of the samples were examined, and the microzone elemental distribution was measured to evaluate the coating wear behavior via a super depth-of-field 3D display system (VHX-2000C, Keyence, Japan) and a scanning electron microscope (S-4800, Hitachi, Japan).

2.3 Wear and corrosion tests

In general, the main factors affecting the wear of materials are load, frequency, temperature, pH, salinity, and conductivity in corrosive solutions [29]. This study investigated the effects of

different surface treatment processes on wear under dry friction and corrosion conditions. As shown in Fig. 5, the schematic of the friction and wear test setup (MS-M9000, Lanzhou Huahui, China) included a friction ball with a diameter of 6 mm made of SiN. The applied loads were 10, 15, and 20 N, with a reciprocating movement frequency of 2 Hz and a displacement amplitude of 5 mm. These test parameters were determined comprehensively on the basis of the actual working conditions of the wind turbine transmission friction pair and the pretests of the samples. In the pretests, no obvious scratches were observed on some coatings under a load of 5 N. Under a load of 10 N, all treated friction pairs exhibited noticeable measurable scratches on their surfaces. At a load of 20 N, paint C experienced delamination. Therefore, a starting load of 10 N was chosen, with test loads of 10, 15, and 20 N selected accordingly. Similarly, the determination of reciprocating frequency, displacement amplitude, and test duration also comes from pretesting. The test time was 40 min, and a 3.5 wt% NaCl solution was used as the medium for the corrosive friction interactive test. In the corrosive friction test, the lower sample was immersed in artificial seawater [30] with an exposed area of 2 cm². Before the test, the sample was left in the solution for 40 min to allow the open-circuit potential (OCP) to stabilize. During the OCP test, the first 20 min before friction and the 20 min after friction were set aside to stabilize the current transient and monitor changes in the OCP on the surface of the samples. The middle 40 min of the test were set to monitor the changes in the OCP and friction coefficient at the same time, and the total test time was 110 min. Throughout the test, the room temperature was maintained at 26 °C. The test parameter design table is shown in Table 1.

3 Results and discussion

3.1 Friction coefficient

By applying the same load, the variation in the friction coefficient for different surface treatment processes can be observed systematically. The results show that the friction coefficients for

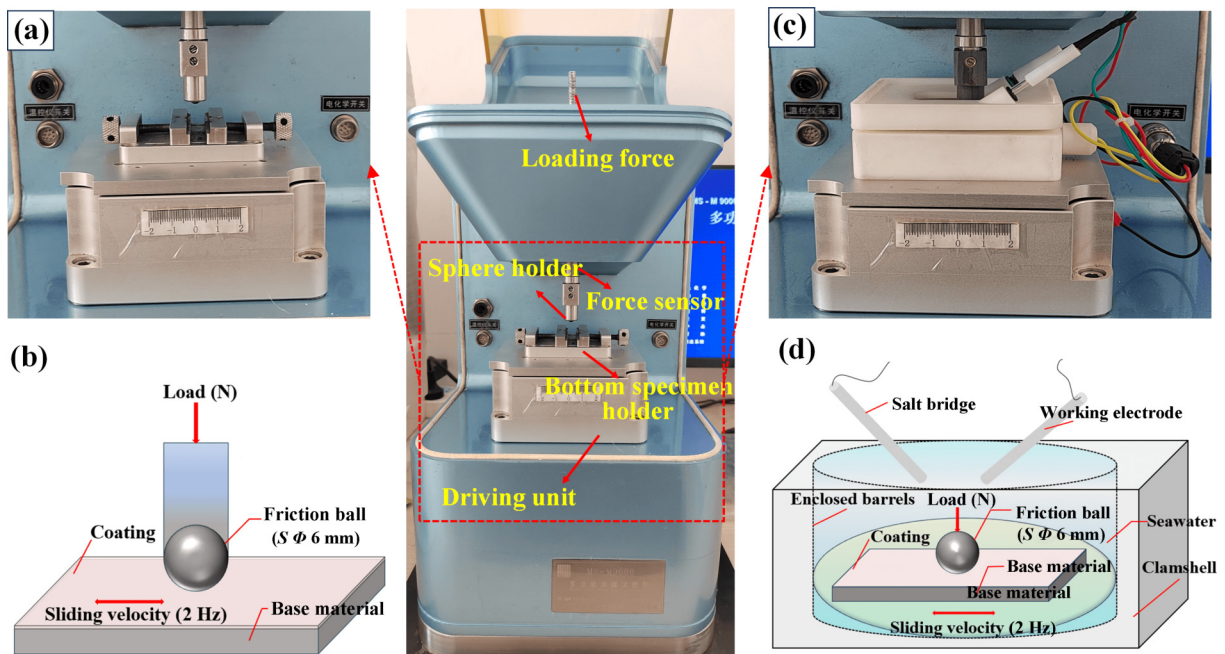


Fig. 5 Schematic diagram of friction-wear test: (a) physical diagram of dry friction conditions, (b) schematic diagram of dry friction conditions, (c) physical diagram of corrosive friction conditions, and (d) schematic diagram of corrosive friction conditions.

various surface treatments follow the mechanism of transition from the running-in stage to the stable wear stage. In the running-in stage, the oxide film formed on the base material in the air medium smooths the contact surface, with friction occurring primarily at the peaks of contact. As the base material is gradually exposed, the friction coefficient increases. During the stable wear stage, the surface smoothness continues to deteriorate, and an oxide film forms continuously. The synergistic effect of these two factors keeps the friction coefficient in a relatively stable state.

As shown in Fig. 6(a), the curves of the friction coefficient versus time for different surface treatment processes indicate that all the curves exhibit an increasing trend followed by stabilization. During the interaction of the friction pairs, the contact type of the surface is elastic-plastic. The friction coefficient decreases as the surface roughness decreases, reaching a minimum friction factor when the surface roughness is $R_a 1.6$.

The friction coefficient variation curve of the coating process shows that the friction coefficients of the different coatings significantly differ. In the zinc-spraying and zinc-plating processes in the run-in phase, the overall trend first increases then decreases, and then increases, and the fluctuation in the process of change is violent. For the curve of the friction coefficient obtained via the

zinc-plating process, the friction coefficient tends to be stable at approximately 20 min, reaching a stable wear stage, with a stable friction coefficient in the range of 0.463–0.475. The friction coefficient change curve of the zinc-spray process tends to stabilize at approximately 25 min and then enters the stable wear stage, with the friction coefficient stabilizing between 0.515 and 0.548. During the spraying process, the zinc powder forms an inhomogeneous cover layer such that the friction coefficient of the surface of the coating increases. Additionally, the distribution of the microconvexities on the surface is not uneven, resulting in many abrasive chips being generated during the friction-wear process, and the discharge of abrasive chips is accompanied by the vibration and jumping phenomenon of the friction pairs, which makes the real contact area change, thus leading to a large fluctuation in the friction coefficient in the stable wear stage of the zinc-spraying process.

For the paint-spraying process, the friction coefficient variation curves of Pb and Pd are roughly the same as those of machining, with the run-in stage completed in a relatively short time, and the friction coefficient stabilized between 0.667–0.681 and 0.577–0.599 in 5 min, respectively. Compared with that of the traditional zinc spraying process, the friction coefficient of the Pb coating increased by 28.4%. The fluctuation of the friction coefficient curve of Pc is relatively special, increasing and then stabilizing. Next, it enters the next rise stage and repeats in a cycle; then, until 30 minutes, it tends toward stable wear, with the friction coefficient finally stabilizing at 0.69–0.7. This phenomenon is mainly due to the occurrence of microexfoliation of the Pc surface during the wear process.

Table 1 Test parameter design table

Grouping	1	2	3
Load F_N (N)	10	15	20
Frequency (Hz)		2	
Environment	Dry friction/3.5% NaCl solution		

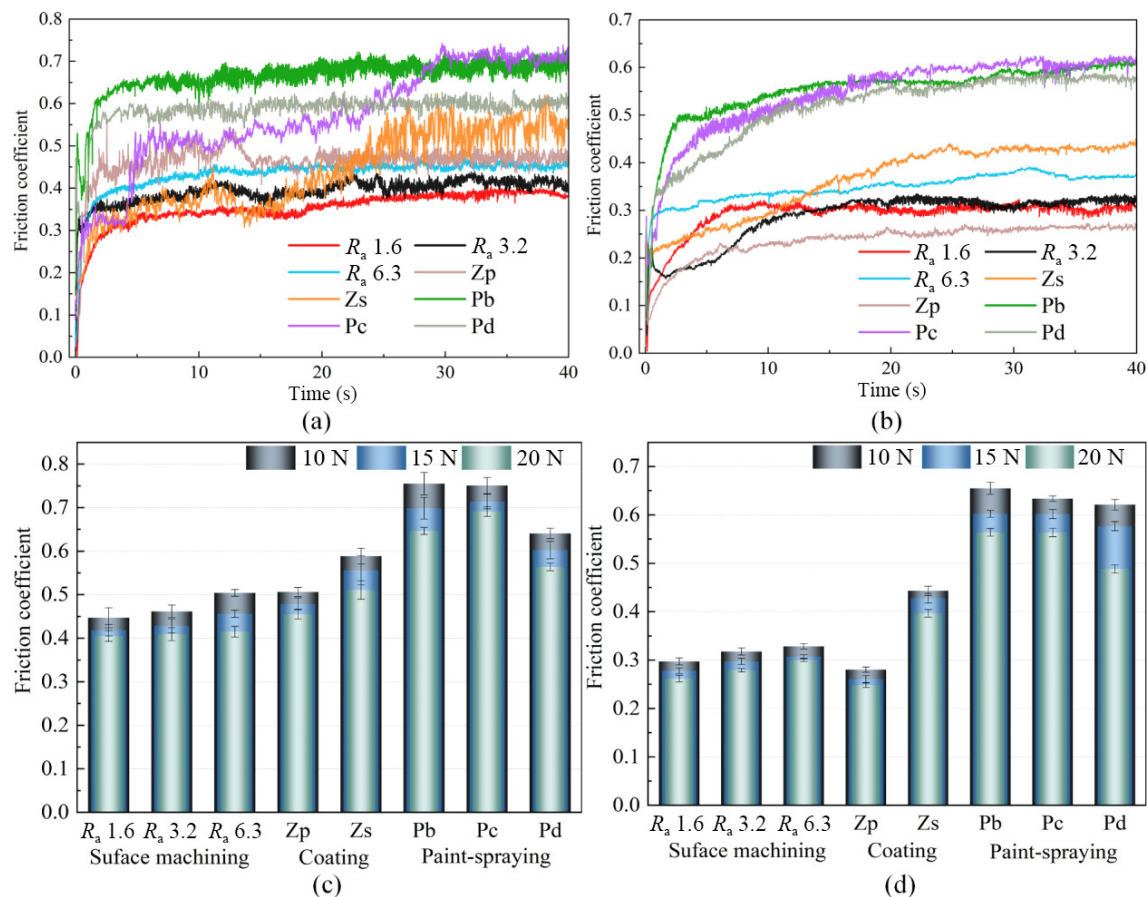


Fig. 6 Friction coefficient variation curve and average friction coefficient: (a) friction coefficient variation curve for dry friction conditions under 15 N load; (b) friction coefficient variation curve for corrosive friction conditions under 15 N load; (c) average friction coefficient for dry friction conditions; (d) average friction coefficient for corrosive friction conditions.

As shown in Fig. 6(b), the friction coefficient variation curves for different surface treatment processes in a corrosive environment under a 15 N load indicate that the friction coefficient is significantly affected by the liquid medium and corrosion products. Generally, the friction coefficient for each process in the corrosive medium is reduced. This phenomenon is attributed to the formation of corrosion products and an oxide film on the friction surface. Notably, after treatment with a 3.5% NaCl solution, many Cl^- and NaCl microcrystals formed on the friction surface. These microcrystals, which can reach nanoscale diameters, are abraded during the wear process and act as solid lubricants [31]. Under the influence of the corrosive medium, the zinc plating process results in the largest change in the stable friction coefficient, reaching a reduction of 45.5%. In contrast, the smallest change occurred in the Pd process, which decreased by only 4.2%, followed by the Pb process, with a decrease of 13.8%. This variation may be due to the zinc-plating process forming a relatively dense oxide film under corrosive conditions [5], which provides a certain lubricating effect [11].

Figures 6(c) and 6(d) show the effects of different load conditions and various surface treatment processes on the average friction coefficient under dry and corrosive friction environments, respectively. The results indicate that the order of friction coefficient levels in the stable state remains consistent across 10, 15, and 20 N load conditions. Further analysis reveals that the stable friction coefficient for each process generally decreases with increasing load. This trend may be attributed to the compression of micro convexities on the surface as the load increases, which, on the one hand, leads to a reduction in surface roughness and frictional resistance. On the other hand, the larger load during continuous friction increases the frictional heat of the material's surface, resulting in softening of the base material and an increase in the real contact area. The combined effects of decreased tangential resistance and increased real contact area contribute to the reduction in the friction coefficient.

On the basis of the analysis of Fig. 6, the order of friction coefficient grades for different surface treatments is as follows: $\text{Pb} > \text{Pc} > \text{Pd} > \text{Zs} > R_a 6.3 > R_a 3.2 > R_a 1.6 > \text{Zp}$. According to previous studies [5], the reason for the highest friction coefficient of Pb is the combined effect of high roughness and high hardness.

3.2 Surface morphology and wear

Figure 7 shows the effects of different loads and surface treatment processes on the wear morphology. The results show that the surfaces of the samples exhibited varying degrees of plastic deformation, with abrasive chip accumulation observed at the ends of the wear marks [32]. A comparison of the surface morphology during the machining process ($R_a 1.6$ – $R_a 6.3$) revealed that the surface hardness increased after machining [6], making it difficult to remove machining marks during the wear process. The greater the surface roughness is, the deeper the machining marks. Owing to the reduced amount of abrasive debris generated during the wear process, which is dominated by the effect of the friction pairs, the wear marks formed on the machined surface are relatively flat and predominantly exhibit V-shaped characteristics.

As shown in Fig. 7, the width and depth of the wear marks from the zinc-spraying process are greater than those from the zinc-plating process, particularly in corrosive media. Notably, compared with those in the machining process, the bottoms of the wear marks in these two coating processes exhibit a pronounced microconvex phenomenon. This may be due to the abrasive debris dislodged from the coating during the wear process being

pushed to the sides of the wear marks, causing concentrated friction at the edges and resulting in reduced friction in the central part of the wear mark, which leads to the formation of a microconvex structure. The same phenomenon is observed in the paint-spraying process.

Compared with the other processes, the paint-spraying process results in a complex and variable wear profile curve, indicating an uneven microconvex structure. With the exception of Pb, the widths of the wear marks for the other two paints are larger, and the edges of the wear marks show a vertical downward trend. This may be due to the adhesive action that causes the paint to peel off in chunks during the wear process. Compared with those of Pc and Pd, the surface characteristics of Pb are bumpy. This can be attributed to the fact that Pb is more viscous and forms undulating pits during the spraying process. These pits lead to an uneven distribution of friction, exacerbating the unevenness of the surface and contributing to its higher friction coefficient.

In addition, during the wear process, Pc and Pd exhibit varying degrees of flaking around the wear marks. Notably, for Pc, under dry friction conditions, the loads of 10 and 15 N do not result in any obvious flaking. However, under a load of 20 N, a small area of flaking of the lacquer layer appears on the surface, which becomes even more pronounced under the influence of corrosive media, causing the lacquer to collapse around the wear marks. This phenomenon indicates that Pc is not suitable for use under larger load conditions and that both Pc and Pd are not suitable for prolonged exposure to a corrosive environment.

Figure 8 compares the changes in the wear amount for different surface treatment processes under dry and corrosive friction conditions. For the transmission connection friction pairs of offshore wind turbine main shafts, the classical surface coating primarily utilizes the zinc-spraying process, with the amount of wear caused by zinc-spraying serving as a reference in this study. The dry friction conditions are shown in Fig. 8(a). Quantitative analysis reveals that the $R_a 1.6$ surface exhibits the best wear resistance, with only 5.00% of the wear occurring during zinc spraying. The $R_a 3.2$ and $R_a 6.3$ surfaces also demonstrate good wear resistance, with wear amounts of 8.90% and 11.50% for the zinc-sprayed samples, respectively. Zinc plating accounts for 38.20% of the wear caused by zinc spraying, which is not as effective as the machining process but still performs reasonably well among the coating processes. The paint-spraying processes (Pb, Pc, and Pd) yield variable results, with the wear resistance of Pb being the best, the wear amount is only 23.80% that of the zinc spraying process, and the wear amount is reduced by 76.20%, whereas Pc and Pd demonstrate relatively poor wear resistance. Notably, Pc has the worst wear resistance, with a wear amount as high as 55.70% for zinc spraying.

The test data indicate that the zinc-spray process results in the greatest amount of wear. This phenomenon is primarily due to the thicker coating formed by the zinc-spraying process and the uneven coating layer on the surface [33]. Compared with the zinc-spray process, the smoother surface texture and lower friction coefficient of the zinc-plating process are key factors contributing to its lower degree of wear. Additionally, the machining process results in the least amount of wear, which is attributed to the hardened layer produced during machining and its low friction coefficient. In contrast, the paint-spraying process (Pb), despite its high friction coefficient, results in less wear than both the zinc-spraying and zinc-plating processes do. This can be attributed to its higher surface hardness and the synergistic effect of zinc powder and paint adhesives.

Figure 8(b) shows the relationships among the wear amount,

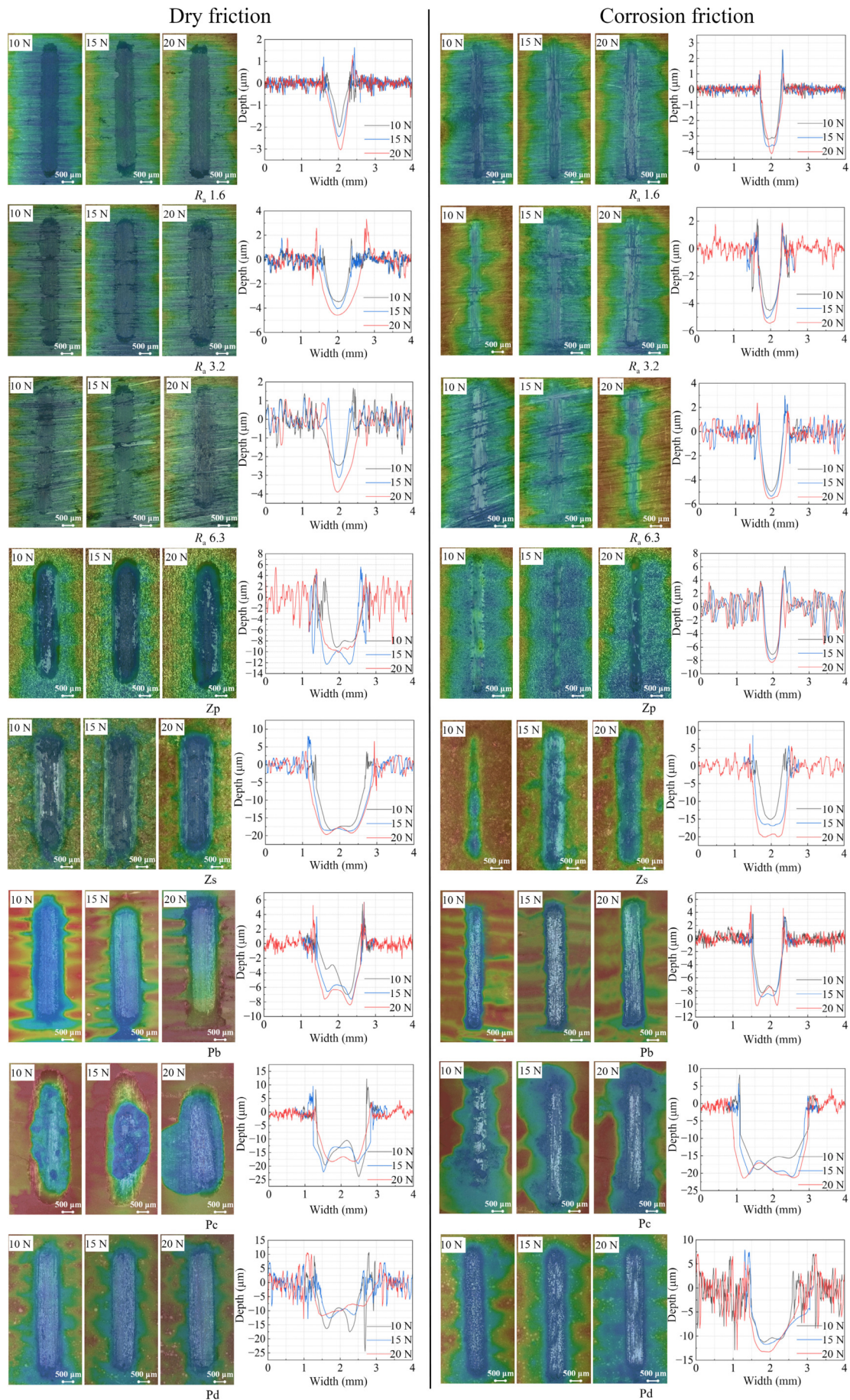


Fig. 7 Wear morphology and wear profile curves for different loads and surface treatment processes.

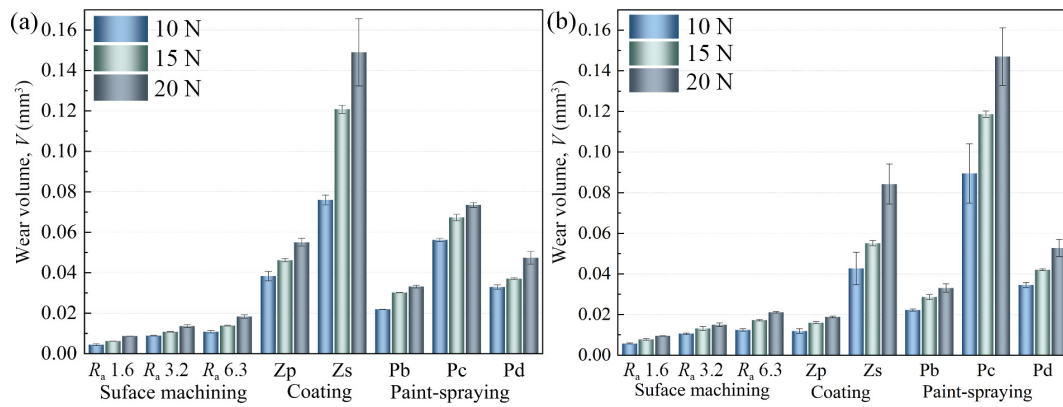


Fig. 8 Comparison of the wear amounts for different loads and different surface treatment processes: (a) dry friction conditions and (b) corrosive friction conditions.

different loads, and various surface treatment processes under corrosive conditions. Similarly, the amount of wear during the zinc-spraying process under a 15 N load is taken as a reference. The quantitative analysis revealed that the R_a 1.6 surface exhibits the best wear resistance, with only 14.08% of the wear amount during the zinc-spraying process. This is followed by R_a 3.2 and R_a 6.3, with wear amounts of 23.79% and 31.25% of the zinc-spraying wear amount, respectively. The wear amount for the zinc-plating process is 29.04% of that of the zinc-spraying process. The wear amount of Pb is 51.90% that of zinc-spraying, whereas the wear amount of Pd is 76.23% that of zinc-spraying. Pc exhibits the worst wear resistance, with a wear amount as high as 215.22% after zinc spraying, which is consistent with dry friction conditions. Analysis indicates that the influence of corrosive media leads to significant flaking and paint ulceration of Pc, which contributes to the noticeable increase in the amount of Pc worn in the corrosive environment.

Figure 9 shows the effects of corrosive media on the wear amount of different surface treatment processes. The results show that the wear amount of Pc in corrosive media significantly increases by 60% to 100% compared with that under dry friction conditions. This phenomenon is primarily due to surface flaking and the fouling of Pc in the corrosive environment. In contrast, Pb is more stable under corrosive conditions, with wear changing by only 3.60% to 13.10% compared with dry friction. Additionally, the corrosive medium negatively affects R_a 1.6, R_a 3.2, R_a 6.3, and Pb (10 N), as well as Pc and Pd. Specifically, under corrosive conditions, the degree of wear of these processes is greater than that under dry friction conditions.

Although the data in Fig. 6 suggest that the friction coefficients decrease in corrosive environments, one might expect the wear amount to be reduced as well. However, the results show the opposite trend, indicating that the effect of corrosion outweighs the benefits of reduced friction coefficients. For the zinc-plating, zinc-spraying, and Pb (15, 20 N) processes, the corrosive media exhibit a positive effect, as the wear amount decreases compared with that of dry friction conditions. This suggests that the reduction in the friction coefficient contributes more to the increase in wear resistance than does the negative impact of the corrosive media. Therefore, the zinc-plating, zinc-spraying, and Pb (15, 20 N) processes can maintain a good level of wear resistance in a corrosive environment.

According to the analysis of Figs. 8 and 9, on the basis of the different surface treatment methods of the friction pairs, the order of the wear resistance levels is as follows: R_a 1.6 > R_a 3.2 > R_a 6.3 > Zp > Pb > Pd > Zs > Pc.

3.3 Electrochemical analysis

Since offshore wind turbines work in high salt spray and corrosive

marine environments, this study also stimulates the seawater environment and analyzes the effects of different surface treatment processes on the change in the OCP of metal samples in a simulated seawater environment in detail. The test results are shown in Fig. 10. The OCP test is first performed before the friction test to ensure the stability of the surface potential of the sample. The OCP measured during friction represents the mixed potential of the unworn and worn areas.

The OCP is an important parameter for evaluating the oxidation resistance and corrosion tendency of metallic materials. According to previous studies [34, 35], a higher OCP of metal

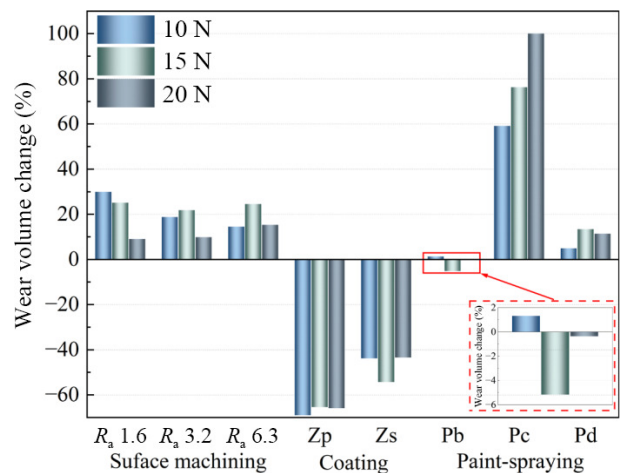


Fig. 9 Wear amount change rates before and after corrosion with different surface treatment processes.

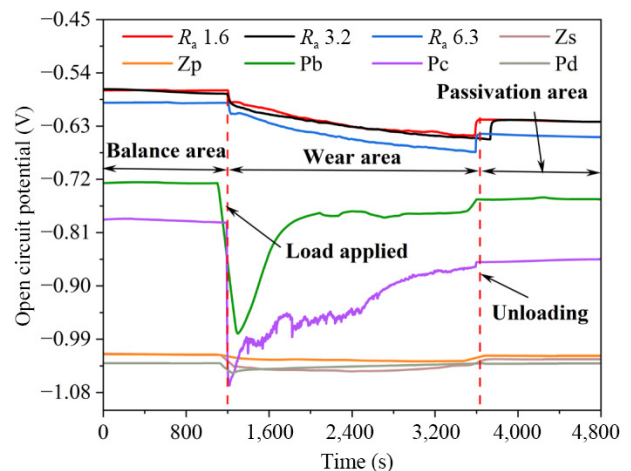


Fig. 10 Variation curves of OCP for different surface treatment processes.

indicates that it is less susceptible to oxidation reactions in its natural state and shows a lower tendency to corrode. Conversely, when the OCP is low, the metal is more susceptible to oxidation reactions and tends to corrode more readily.

The test results show that the OCP in the balanced area of the machining process (R_a 1.6– R_a 6.3) is stable at approximately -0.55 V, and the OCP of R_a 6.3 is lower than those of R_a 1.6 and R_a 3.2. This suggests that the anticorrosion properties of the machining process are affected by different surface roughness levels. The higher the roughness is, the lower the OCP, indicating a greater tendency toward corrosion and weaker anticorrosion performance. The anticorrosion levels are ranked as R_a 1.6 > R_a 3.2 > R_a 6.3.

The OCP in the balanced area of the zinc-spraying and zinc-plating processes is relatively consistent, remaining stable at approximately -1 V, indicating that the anticorrosion properties of the samples treated by these two processes are not significantly different. However, there is a notable difference in the OCP of the paint-spray process, with the OCP values for Pb, Pc, and Pd being -0.72 , -0.78 , and -1 V, respectively. These findings indicate that the type of paint has a greater effect on the anticorrosion properties of the samples. The anticorrosion levels for the paint-spraying process are ranked as Pb > Pc > Pd.

After the OCP stabilizes for 20 min, a load is applied for sliding friction. The test data show that the OCP of the wear region decreases sharply. This occurred because the applied load destroyed the original passivation film on the sample surface, exposing the fresh active surface to the corrosive solution and triggering galvanic coupling corrosion. Moreover, damage to the passivation film increases the anodic reaction, causing the surrounding surfaces to undergo organizational polarization [36]. As wear intensifies, the OCPs of the other processes, with the exception of the spray painting process, slowly decrease. This may be due to continuous friction increasing the active area of the worn track, leading to an electric potential imbalance and causing changes in the OCP.

For the paint-spraying process, after an initial decrease to a specific value, the potential tends to increase as wear continues. This indicates that during the wear process, the rate of fresh surface production on the coating is lower than the rate of surface passivation, and the passivation film plays a role in corrosion prevention. Especially for Pb, during the wear process, its OCP decreases and quickly recovers, indicating that the passivation film of this coating has good self-healing ability, making the surface more stable and less prone to oxidative corrosion. The potential change results from the dynamic equilibrium between the destruction and repair of the passivation film on the sample surface [37]. After the end of sliding friction, each sample enters the passivation area, and the OCP increases rapidly within a short period, reaching a relatively stable state due to the repassivation reaction occurring on the surface of the sample.

In this study, after different surface treatments, the equilibrium potentials of the samples are highest for the machining process, followed by the paint-spraying process and zinc-coating process (zinc spraying and zinc plating). Both the paint-spraying and zinc-coating processes are based on zinc powder. Since the OCP of zinc is more negative than that of steel, after coating treatment, zinc will form a more negative anodic potential on the steel surface. Therefore, in a corrosive environment, these coatings are more likely to corrode, thereby protecting the steel base material from corrosion. Although the surfaces of the machining process exhibit high OCPs and theoretically have a lower tendency to corrode, offshore wind turbines are subjected to extreme conditions such

as high salt spray, high humidity, and corrosive atmospheres, which increase the susceptibility of the base material to oxidative corrosion. This can potentially lead to the failure of transmission components; therefore, treating friction pairs with machining alone will not be sufficient to provide long-term protection.

3.4 Wear mechanism

As shown in Fig. 11(a), the oxygen (O) atom content in the R_a 1.6 abrasive chip accumulation area is greater than that in the abrasive scar area. This may be due to the base material reacting with oxygen atoms in the air during the wear process, forming fine oxides. With relative motion, these fine oxides accumulate at the end of the wear marks, resulting in oxide build-up. Simultaneously, the abrasive particles create fine scratches and pits in the wear area. This suggests that the main form of wear on the R_a 1.6 surface is abrasive wear [38]. Figure 11(b) shows phenomena such as plastic tearing, spalling pits, and fine scratches on the abraded surface of R_a 3.2, possibly due to the formation of larger wear particles during the wear process. The primary forms of wear on the R_a 3.2 surface are abrasive grain wear and adhesive wear [39]. Figure 11(c) indicates that the elemental content in the area of abrasive build-up on the R_a 6.3 surface is similar to that of R_a 1.6, but the scratches are more pronounced. This may be caused by larger wear particles forming during the wear process, leading to plowing and more prominent cutting craters. The main forms of wear on the R_a 6.3 surface are abrasive and adhesive wear.

The wear surfaces during the zinc-plating and zinc-spraying processes are shown in Figs. 11(d) and Fig. 11(e), respectively. The wear surface of the zinc-plating process clearly exhibits flaking pits and numerous wear particles, which mainly consist of Zn atoms and partially formed ZnO particles. Additionally, plowing and cracking phenomena occur due to the action of abrasive particles, so the primary forms of surface wear for the zinc-plating process are abrasive and fatigued wear [40]. In contrast, the wear surface of the zinc-spray process does not exhibit obvious spalling pits, and the scratches are finer; however, numerous cracks and white oxide layers are present. Moreover, during the wear process, the oxides are not discharged promptly with relative motion, resulting in oxide bumps. The analysis indicates that the wear forms for both the zinc-spraying and zinc-plating processes are similar.

The ESD images of the wear areas of the paint-spraying process are shown in Figs. 11(f)–11(h). As depicted in Fig. 11(f), the surface of the wear marks on Pb is relatively smooth. The wear marks are characterized mainly by plowing, and the primary wear mechanism for Pb is abrasive grain wear. In contrast, the wear surface of Pc clearly exhibits cracks and varying degrees of plastic tearing, indicating that both the hardness and adhesion of Pc are poor. The main wear mechanisms of Pc are abrasive wear, adhesive wear, and surface fatigue wear. As shown in Fig. 11(h), the wear area of Pd is dominated by Fe, which suggests that most of the coating has worn off, leaving only a few Zn atomic particles on the surface, while oxidation of the base material has occurred. Compared with the other two types of paint-spraying processes, Pd has the poorest adhesion and wear resistance. The main wear mechanisms of Pd include abrasive grain wear, adhesive wear, surface fatigue wear, and erosive wear.

Figures 12(a)–12(c) show the ESD images of the wear areas of the surface machining processes under corrosive friction conditions. From the observations, it can be concluded that, compared with dry friction conditions, the presence of corrosive media results in flatter wear areas, with fine scratches evolving into more pronounced plowing and pitting craters appearing to

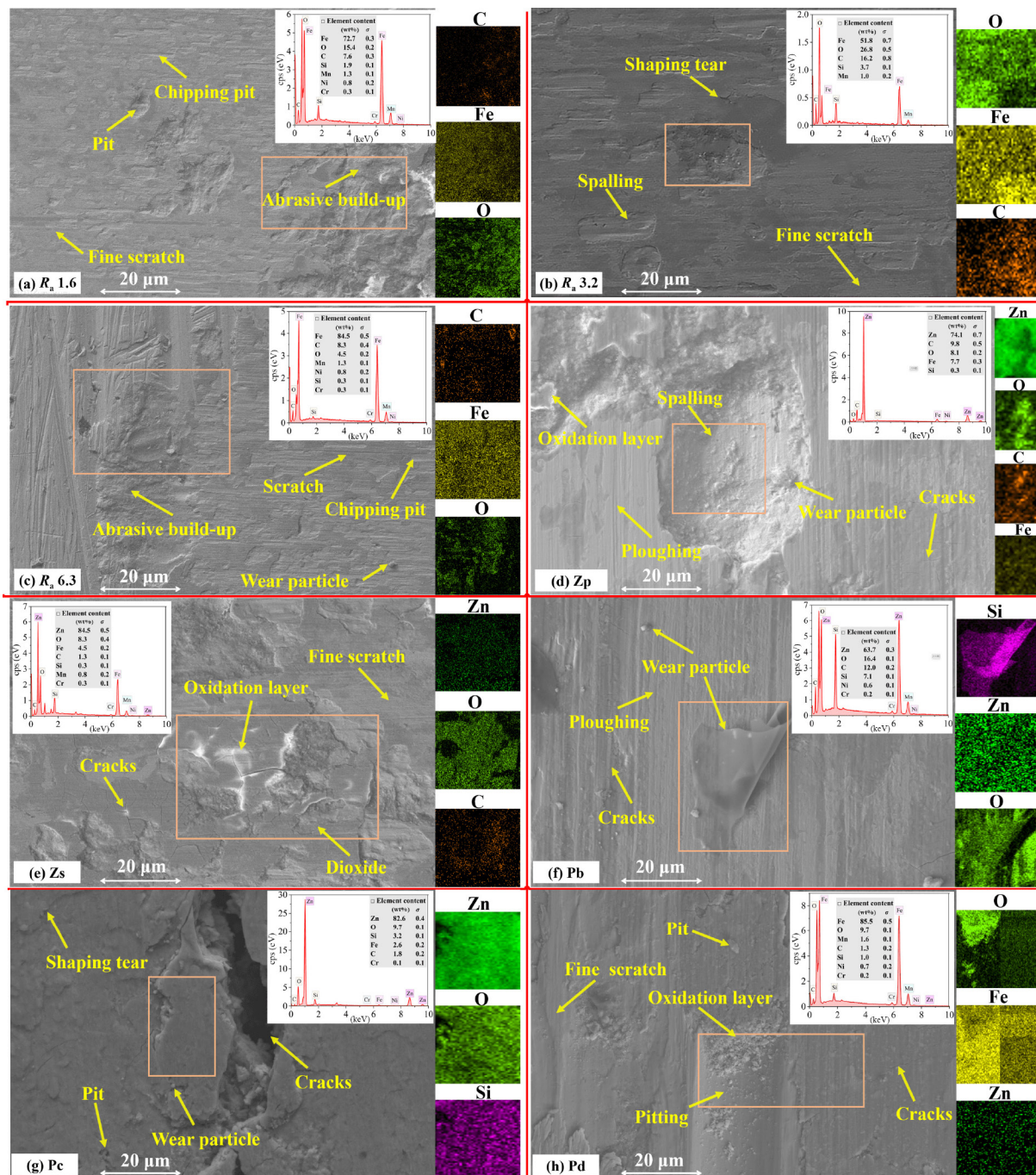


Fig. 11 ESD scanning images of different surface treatment processes and distributions of important elements under dry friction conditions with a 15 N load.

varying degrees. Notably, more severe oxide attachment occurs on the surface of R_a 3.2, forming oxide fragments, and the primary wear mechanisms are abrasive wear and corrosion wear.

As shown in Figs. 12(d) and 12(e), the wear morphologies of the samples subjected to the zinc-plating and zinc-spraying processes under corrosive conditions are compared. In contrast to dry friction conditions, the zinc-plating process does not result in obvious spalling craters, possibly due to a lubrication effect, which allows wear particles to be discharged from the wear area more easily, preventing severe physical damage. However, the surfaces of the wear marks exhibit more severe oxide build-up and pockmarks. For the zinc-spray process, the corrosive environment leads to the formation of a white oxide layer, which is more pronounced than that under dry friction conditions, and the

surface displays more pitting. The primary wear mechanisms for both the zinc-spraying and zinc-plating processes are abrasive wear and corrosive wear.

Figures 12(f)–12(h) show the ESD images of the wear areas of the paint-spraying process under corrosive conditions. Figure 12(f) shows that, due to the corrosive medium, flaking occurs on the surface of Pb, and both the flaked area and the normal wear area appear as fault zones. At the same time, the normal wear area, similar to the dry friction conditions, exhibited plowing and microcracks but formed more lumpy oxidized regions with a darker surface color. Through analysis, it can be observed that the wear forms of Pb are primarily abrasive wear, surface fatigue wear, and corrosion wear. From the analysis of the elemental map on the surface of the wear marks, it is evident that the Pc and

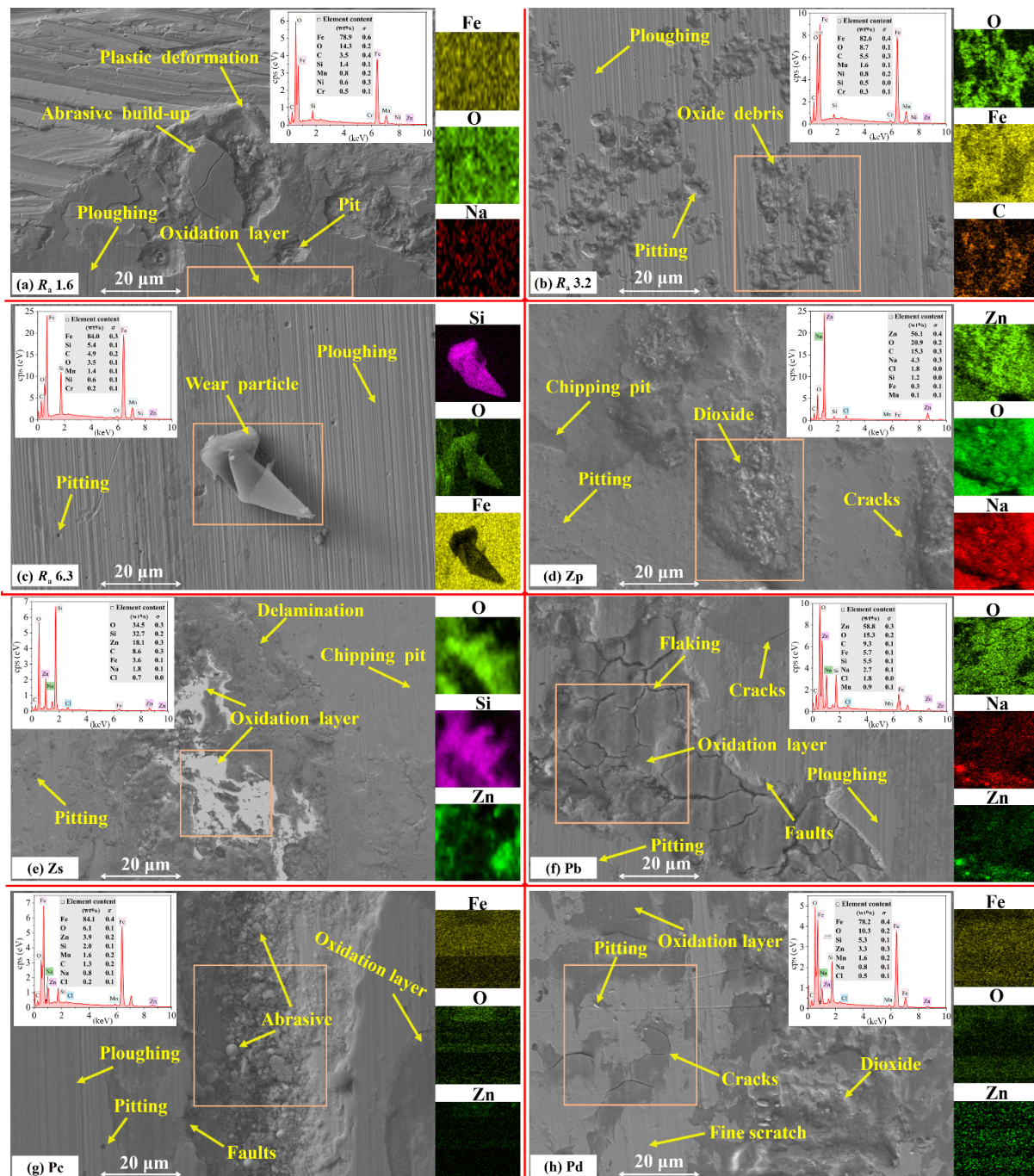


Fig. 12 ESD scanning images and distribution of important elements of different surface treatment processes under corrosive friction conditions with a 15 N load.

Pd processes experience large areas of spalling during wear. The wear surfaces show large spalling craters, accumulation of internal abrasive debris, prominent oxide layers, and cracks. Therefore, the main wear forms of Pc and Pd are abrasive wear, surface fatigue wear, corrosion wear, and erosive wear.

3.5 Wear resistance and anticorrosion mechanism

The wear resistance and anticorrosion mechanisms of the different surface treatment processes are illustrated in Fig. 13. In terms of tribological properties, surface hardness, roughness, and abrasive debris are key factors influencing the wear resistance of a material. A high-hardness surface effectively resists external forces, reducing plastic deformation and material spalling, thus minimizing wear. The micro-protrusions on surfaces with high roughness, when subjected to concentrated loads, lead to an

increase in local contact stresses, which accelerates the plastic deformation and fracture of the material, resulting in more severe wear. Furthermore, abrasive particles, such as hard debris, form a three-body wear mechanism with friction pairs, causing increased microcutting, plowing, and surface scratches, thereby intensifying the wear process [41].

The machining process achieves optimal wear resistance by increasing the hardness of the base material [6]. According to the hardness results in Fig. 4, the hardness values of R_a 1.6 to R_a 6.3 are similar. Combined with the wear statistics in Fig. 8, it is evident that the difference in wear resistance among the various machining processes primarily depends on surface roughness. The lower the roughness is, the less wear occurs, leading to better wear resistance. The surface hardnesses of the zinc-spraying and zinc-plating processes are similar; however, the sprayed surface is

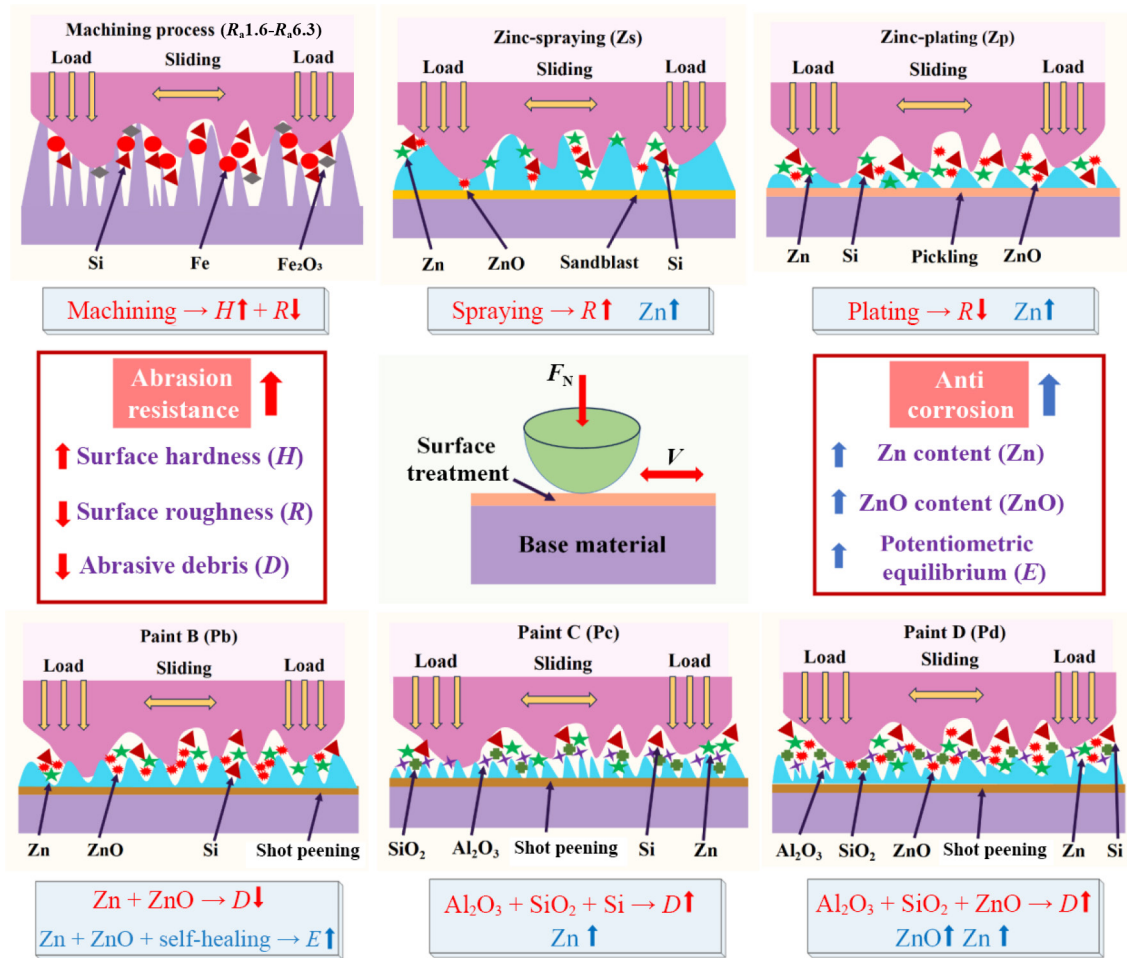


Fig. 13 Wear resistance and anticorrosion mechanisms of different surface treatment processes.

uneven and has greater roughness, whereas the electroplated surface is smoother and has lower roughness, resulting in poorer wear resistance for zinc-spraying. The wear resistance of the paint-spray process mainly depends on the type of adhesive used. The adhesives in Pc and Pd are predominantly Al_2O_3 and SiO_2 , which generate a significant amount of hard abrasive debris during the wear process. This abrasive debris forms a three-body wear mechanism with friction pairs, resulting in poor wear resistance for Pc and Pd. In contrast, the adhesive in Pb is primarily ZnO, which works synergistically with Zn powder, producing less abrasive debris and forming a micro/nanoparticle self-lubricating mechanism [42], thus enhancing the wear resistance of the coating.

In terms of anticorrosion, the protection of the base material surface is effectively enhanced by sacrificial anodes. Zinc, as an active metal, preferentially reacts in corrosive environments and forms a dense oxide layer (passivation film) that isolates the corrosive medium, providing protective benefits. The zinc-spraying, zinc-plating, and paint-spraying processes all significantly reduce the corrosion rate of the base material. Additionally, under corrosive conditions, Pb undergoes an oxidation reaction, generating ZnO from Zn^{2+} , which promotes the redeposition and recrystallization of the ZnO adhesive, thereby forming a self-healing mechanism for the passivation film. The passivation protection capability of the Pb passivation film is stronger than that of other coatings, leading to a rapid increase in potentiometric equilibrium, which reduces the occurrence of corrosion reactions and enhances anticorrosion performance.

As shown in Table 2, to determine the optimal surface

treatment process, the recommended order for treating the transmission connection friction pairs of offshore wind turbine main shafts is presented. This order integrates the wear morphology, friction coefficients, wear amounts, changes in wear rates before and after corrosion, electrochemical properties, and wear mechanisms identified from the friction-wear tests: $Pb > Zs > Pc > Pd > Zp > R_a 1.6 > R_a 3.2 > R_a 6.3$.

The machining process ($R_a 1.6-R_a 6.3$) results in good wear resistance; however, its friction coefficient and anticorrosion properties are lacking. Therefore, it is not advisable to rely solely on machining for the surface treatment of the transmission connection friction pairs. The wear resistance of zinc plating is comparable to that of machining, but its lower friction coefficient fails to meet the operational requirements for transmitting large torques in wind turbines, making it unsuitable. Additionally, Pc and Pd are not recommended as surface coatings for friction pairs because of their poor adhesion, shear resistance, and significant flaking under corrosive conditions, leading to inadequate wear resistance. In contrast, Pb not only has a high friction coefficient that meets the requirements for large torque transmission in offshore wind turbines but also offers good wear and corrosion

Table 2 Order of friction behavior levels

Behavior	Preferred grade order
Friction coefficient	$Pb > Pc > Pd > Zs > R_a 6.3 > R_a 3.2 > R_a 1.6 > Zp$
Wear-resistance	$R_a 1.6 > R_a 3.2 > R_a 6.3 > Zp > Pb > Pd > Zs > Pc$
Anti-corrosion	$Pb > Pc > Zp \geq Zs > Pd > R_a 1.6 > R_a 3.2 > R_a 6.3$

resistance. Considering the environmental pollution associated with the zinc-spraying process, the use of Pb instead of traditional zinc-spraying as the preferred coating for the transmission connection friction pairs of offshore wind turbine main shafts is recommended.

4 Wear prediction

4.1 Theoretical model of ball-and-disc wear

Considering the poor anticorrosion properties of the machining process, this study focuses on the wear prediction of coating processes, including zinc spraying, zinc plating, and paint spraying. Through the analysis of the wear mechanisms of these coating processes, the main wear forms of the friction pairs are identified as abrasive wear, adhesive wear, fatigue wear, and corrosion wear.

The presence of a certain degree of roughness on the material surface of the friction pair indicates that the real contact area is smaller than the nominal contact area. From the microscopic perspective of abrasive wear, adhesive wear, and fatigue wear, each micro convexity influences the macroscopic wear behavior. The size and distribution of the real contact area play a decisive role in wear. As wear progresses, the real contact area changes, resulting in changes in the contact pressure. Therefore, the theoretical model of ball-disc wear is established by considering that the contact of the friction pair surfaces occurs on conical microconvex surfaces of their respective unique height h , cone-bottom diameter $2r$, and same cone-bottom angle θ , whereas the number of contacts at the contact points on each of the contact surfaces under consideration is n , and each of these microconvex surfaces forms a conical wear chip as it slides.

On the basis of the above, the geometric relationship gives the microconvex height $h = r \tan \theta$; the smoother the surface is, the smaller the θ angle and the smaller $\tan \theta$ is. The load on each contact point is $w = \pi r^2 \sigma_s$, where σ_s is the yield strength. The total wear amount V and total load W can be expressed as Eqs. (1) and (2) [43]:

$$V = Lq \quad (1)$$

$$W = \sum w = n\pi r^2 \sigma_s \quad (2)$$

where L is the sliding distance of the conical microconvex and q is the volumetric wear rate of a microbump over a distance of $2r$ in diameter at the base of the cone.

When the sliding distance is $2r$, the volume Δv of the sheared conical microconvex and the volumetric wear rate q are as Eqs. (3) and (4) [44]:

$$\Delta v = 1/3\pi r^2 h \quad (3)$$

$$q = \Delta v/2r = \pi r h/6 \quad (4)$$

The total amount of wear V at a distance of sliding L is as Eq. (5):

$$V = Lq = \sum \pi r h L/6 = n\pi L r^2 \tan \theta/6 \quad (5)$$

From Eqs. (2) and (5), the total amount of wear V about the load at the sliding L distance can be obtained (Eq. (6)):

$$V = L \sum_0^n q = n\pi L r^2 \tan \theta/6 = WL \tan \theta/6\sigma_s \quad (6)$$

Here, the yield strength σ_s is replaced by the material hardness

H , assuming that $H = k_0 \sigma_s$. k_0 is the scale factor of material hardness and yield strength. Then, Eq. (6) can be changed to Eq. (7):

$$V = L \sum_0^n q = \frac{n\pi L r^2 \tan \theta}{6} = \frac{WL}{6k_0 H} \tan \theta \quad (7)$$

In the actual friction-wear process, the microconvex contact does not always produce abrasive debris; thus, it can be assumed that the microconvex contact with probability constant k_1 produces abrasive debris. Moreover, in the friction corrosion test, the addition of corrosive media affects the amount of wear, so the corrosion coefficient is introduced to represent the impact of the corrosive media on the degree of wear. Assuming that the corrosion wear coefficient is k_c , then:

$$V = k_1 k_c L \sum_0^n q = k_1 k_c \frac{n\pi L r^2 \tan \theta}{6} = k_1 k_c \frac{WL}{6k_0 H} \tan \theta \quad (8)$$

For the convenience of data processing and simulation calculations, all the coefficients are simplified to wear coefficients K , which can be obtained as

$$V = k_1 k_c \frac{WL}{6k_0 H} \tan \theta = K \frac{WL}{H} \quad (9)$$

The wear coefficient K is related mainly to the surface roughness, surface conditions of the material, and corrosive media; under dry friction conditions, the corrosive wear factor k_c does not contribute to the volumetric wear, so it can be assumed that $k_c = 1$, and the wear coefficients under dry and corrosive friction conditions are K_1 and K_2 , respectively.

Equation (9) is consistent with the form of the ARCHARD adhesive wear theory model [45]. To simulate the evolution process of the contact surface with wear time, it is necessary to identify the wear depth at each contact node of the contact surface of the finite element model and convert the wear amount into the wear depth. When the contact area ΔA and the time increment dt are infinitesimal, the differential form can be expressed as Eqs. (10) and (11):

$$dV = A dh = \frac{KW}{H} dL = \frac{KP}{H} v dt \quad (10)$$

$$dh = \frac{KP}{H} v dt \quad (11)$$

where dh is the wear depth in dt time, A is the real contact area, P is the contact pressure, and v is the sliding speed.

During wear simulation, the need for constant iterative computation results in a large time increment, so the computational efficiency can be improved by using appropriate incremental techniques. An automatic variable increment technique is used here after considering the threshold wear depth for the maximum allowable local wear increment, i.e., the wear depth is calculated on the basis of the current increment time automatically selected by the finite element software. If the wear depth is greater than a predefined threshold, the algorithm stops the current increment and uses it to select another increment time. The local wear depth for increment i is obtained from Eq. (11):

$$dh_i = \frac{KP}{H} v dt_i \quad (12)$$

Considering dh_{\max} as the maximum permissible local wear increment, dh_i must be less than dh_{\max} . If $dh_i > dh_{\max}$, then $dh_i = dh_{\max}$. Therefore, the new increment time dt_{in} is as Eq. (13):

$$dt_{in} = dt_i \frac{dh_{max}}{dh_i} \tag{13}$$

As the contact surface wears, the real contact area changes, resulting in the contact pressure also changing. Therefore, a sufficient number of increments must be considered to obtain a more realistic wear model, and the total wear depth for the i th increment is as Eq. (14):

$$h_i = h_{i-1} + dh_i = \sum_0^{i-1} \frac{KP}{H} v dt + \frac{KP}{H} v dt_i \tag{14}$$

where h_i is the total wear depth of the i th increment, h_{i-1} is the total wear depth of the i th increment, and dh_i is the wear depth of the current increment.

4.2 Finite element modeling and analysis of results

A ball-disc model is established via ABAQUS finite element software, and several steps, such as material setting, load application, boundary condition setting, and meshing, are completed. The 3D assembly model is shown in Fig. 14(a). To simulate the wear process more accurately, the ALE adaptive mesh technique is introduced. As shown in Fig. 14(b), the total number of grids is 44,160, with the size of the mesh refinement area meeting the requirements of 2 mm × 10 mm × 3 mm; the number of grids in this area is 9,600. Real-time updating of the model mesh through the created ALE adaptive mesh is achieved, ensuring that during the simulation process, the stress is updated before the amount of wear for each load increment is calculated.

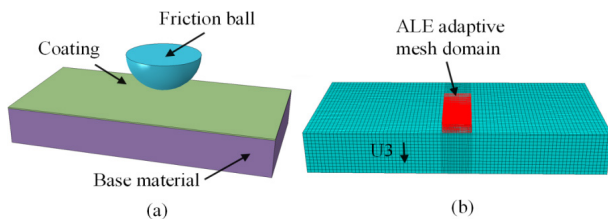


Fig. 14 3D assembly model with ALE adaptive mesh region.

Moreover, the UMESHMOTION subroutine is developed, which is based mainly on the wear theory model of the ball-disc friction pair proposed in the previous section. Finally, the amount of wear is measured through testing, and the wear coefficient is calculated on the basis of the theoretical model.

The wear coefficient considers the influence of actual contact coating surface roughness, the environment, and corrosion on the amount of wear. The influencing factors are simplified as the wear coefficient for finite element calculations, effectively solving the problem of difficult convergence of fluid-structure coupling in finite element simulations under corrosive media and improving the calculation efficiency. In the actual test, the wear time was 40 min. To ensure the calculation efficiency and accuracy of the simulation, the incremental step time is set to 24 s, and the total wear depth is $h_{tot} = 100 \times \Delta\Sigma h$, which can be obtained from a wear depth of 40 min.

Finite element simulation of the wear depth is conducted via the ball-disc wear model established above, with the wear direction set to U3. By simulating the removal of material from the surface of the coating and measuring the displacement in the U3 direction after wear, the depth of wear on the surface of the coating can be obtained. On the basis of the arbitrary Lagrangian-Eulerian (ALE) adaptive grid and the UMESHMOTION subroutine, real-time updates of the contact pressure and wear depth are achieved. Combined with the simulation step size, the overall wear amount is solved iteratively.

4.2.1 Dry friction conditions

As shown in Fig. 15, under dry friction conditions, the wear amounts obtained from the finite element simulation compared with the test wear amounts indicate that zinc-spraying has the greatest amount of wear, whereas Pb has the smallest amount. The trends are consistent. Under the 10 N loading condition for Pb, the minimum error between the simulated and test wear results is 0.5%, which indicates that the simulation data can be considered equivalent to the test data. In contrast, under the 10 N loading condition for Pc, the maximum error between the simulated and test results is 5.8%.

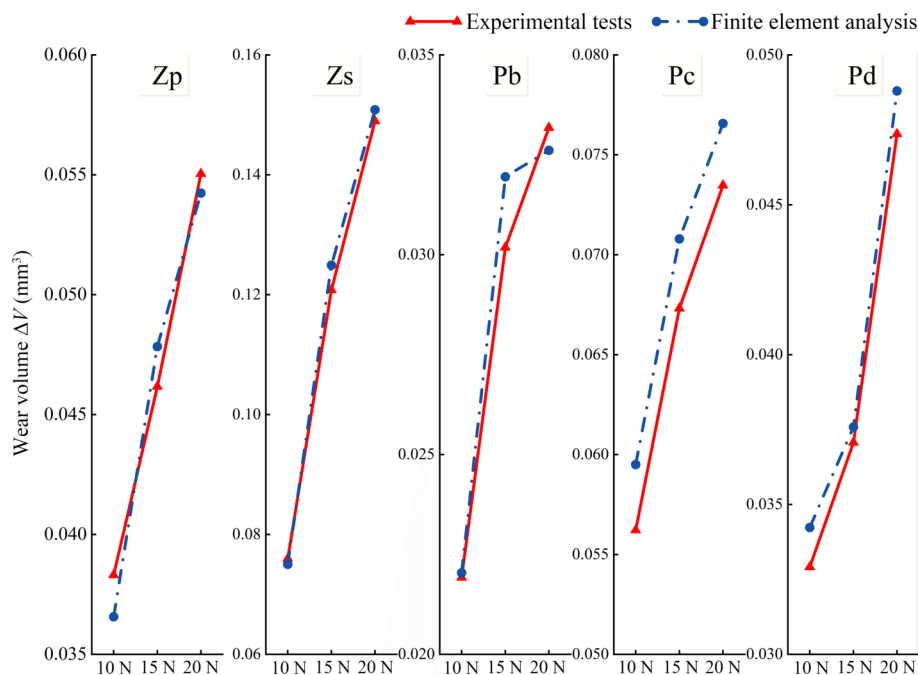


Fig. 15 Test and simulated wear under dry friction conditions.

4.2.2 Corrosive friction conditions

The simulation analysis for the corrosive friction conditions is based on the same model as that for the dry friction conditions, with the key difference being the adjustment of the wear coefficient. According to the analysis of the wear mechanism, owing to the influence of corrosive media, the wear mechanism includes not only abrasive, adhesive, and fatigue wear but also corrosive wear. By analyzing the wear theory model, this study considers the influence of corrosive media on wear through the corrosion coefficient k_c . Then, according to the specific situation in the corrosive environment, the wear coefficient k_c is introduced to adjust the wear coefficient K of the model, and it is written into the UMESHMOTION subroutine to simulate the wear behavior of the model under corrosive conditions.

The specific data for the corrosive conditions are shown in Fig. 16, where it can be observed that for Pc under a 10 N load, the maximum error of 6.26% is recorded between the simulated and

test wear. Notably, Pc has the maximum error value under both dry and corrosive friction conditions. According to the surface wear morphology in Fig. 7, during the test, Pc shows varying degrees of paint peeling and festering phenomena, which accounts for the significant discrepancy between the simulation results and the test results. Pd achieves a minimum error of 0.93% between the simulated and test wear amounts at a 15 N load. The comparison indicates that the difference between the simulated and test wear is greater for the corrosive conditions than for the dry friction conditions, suggesting that the corrosive environment increases the uncertainty between the simulation and testing. Moreover, in establishing the simulation model, the influences of actual contact surface roughness, the environment, and corrosion on the volume of wear are considered through the wear coefficients. Compared with dry friction conditions, more factors influence the amount of wear in corrosive environments, which may explain the significant error between the simulation results and the test results.

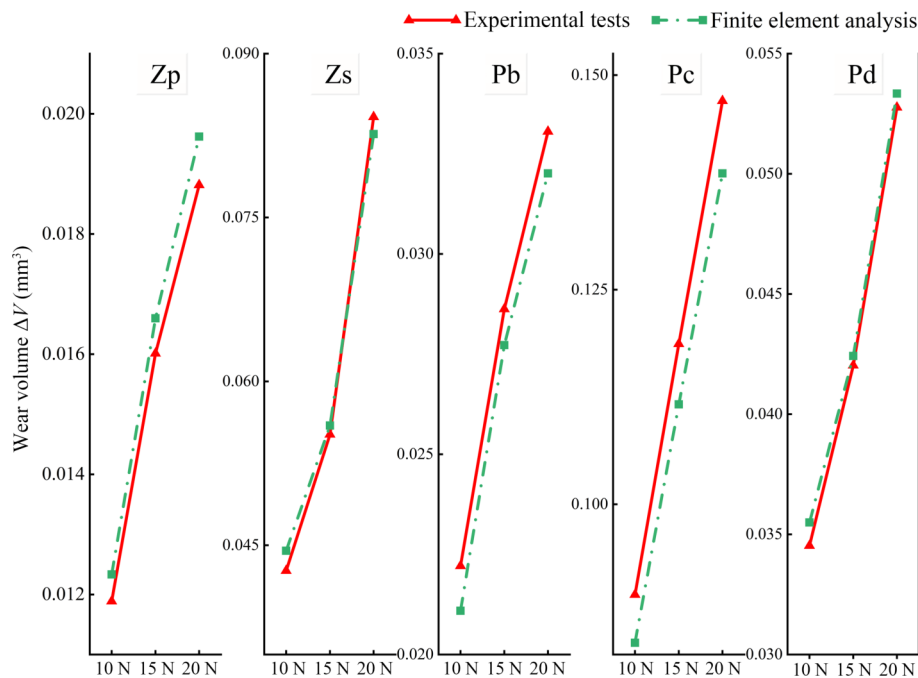


Fig. 16 Test and simulated wear under corrosive friction conditions.

In summary, under both dry friction and corrosive friction conditions, the maximum error in wear between the finite element calculation and experimental test results is only 6.26%, which verifies the accuracy of the wear theory model, thus guiding the precise design of transmission friction pairs for wind turbines.

5 Conclusions

Using the transmission connection friction pairs for the main shaft of offshore wind turbines as a case study, the wear resistance and anticorrosion mechanisms of the friction pairs with different surface treatment processes are examined. The main conclusions are as follows:

(1) Interzinc B paint has comprehensive friction-wear and anticorrosion behavior, among which a rough and high-hardness surface increases the friction coefficient and ensures high torque transmission requirements. The wear resistance benefits from the synergistic effect of the Zn powder and ZnO adhesive, which produces less abrasive debris and forms a micro/nanoparticle self-

lubricating mechanism. The anticorrosion effect is attributed to the self-healing mechanism of the passivation film, where Zn^{2+} undergoes oxidation to generate ZnO, promoting the redeposition and recrystallization of the ZnO adhesive. This self-healing coating reduces corrosion reactions.

(2) The machining process achieves optimal wear resistance by increasing the hardness of the base material. The surface hardness of the zinc-plating and zinc-spraying processes is similar; however, the uneven coating layer on the zinc-spraying surface leads to reduced wear resistance. The adhesives Al_2O_3 and SiO_2 in the paints of brands Hempel C and Interzinc D form a three-body wear mechanism with friction pairs, resulting in poor wear resistance for both paints.

(3) Instead of the classical zinc-spraying process, paint from the brand Interzinc B is recommended as the coating material for the transmission connection friction pairs of offshore wind turbine main shafts. This coating not only meets the high friction coefficient requirements of friction pairs but also results in better wear resistance and anticorrosion properties.

(4) To predict coating wear, a theoretical ball-disc wear model with dynamic changes in the contact area during the wear process is established. The wear amounts of different coatings under dry and corrosive friction conditions are dynamically simulated via finite element secondary development. The maximum error between the comparative test results is controlled at 6.26%, verifying the feasibility of the theoretical wear model.

Acknowledgements

This study was supported by the National Natural Science Foundation of China (No. 51875382), the Fundamental Research Program of Shanxi Province (No. 202203021222206), the Scientific and Technological Innovation Programs of Higher Education Institutions in Shanxi (No. 2022L275), the Research startup fund project of Taiyuan University of Science and Technology (No. 20222048), and the Outstanding doctoral award fund for coming to Jin (No. 20232050).

Declaration of competing interest

The authors have no competing interests to declare that are relevant to the content of this article.

References

- [1] Momber A W, Nattkemper T W, Langenkämper D, Möller T, Brün D, Schaumann P, Shojai S. A data-based model for condition monitoring and maintenance planning for protective coating systems for wind tower structures. *Renew Energ* **186**: 957–973 (2022)
- [2] Pei W L, Pei X L, Xie Z Z, Wang J M. Research progress of marine anti-corrosion and wear-resistant coating. *Tribol Int* **198**: 109864 (2024)
- [3] Greco A, Sheng S, Keller J, Erdemir A. Material wear and fatigue in wind turbine systems. *Wear* **302**(1–2): 1583–1591 (2013)
- [4] Zhang B B, Wang J Z, Liu H, Yan Y F, Jiang P F, Yan F Y. Tribocorrosion properties of AISI 1045 and AISI 2205 steels in seawater: Synergistic interactions of wear and corrosion. *Friction* **9**(5): 929–940 (2021)
- [5] Ning K, Wang J M, Shi M J, Ning W G, Zhang F. Friction-increasing mechanism of contact pair using different surface treatment processes. *Tribol Int* **165**: 107337 (2022)
- [6] Zhai W, Bai L, Zhou R, Fan X, Kang G, Liu Y, Zhou K. Recent progress on wear-resistant materials: Designs, properties, and applications. *Adv Sci* **8**(11): 2003739 (2021)
- [7] Price S J, Figueira R B. Corrosion protection systems and fatigue corrosion in offshore wind structures: Current status and future perspectives. *Coatings* **7**(2): 25 (2017)
- [8] Lee C K. Corrosion and wear-corrosion resistance properties of electroless Ni–P coatings on GFRP composite in wind turbine blades. *Surf Coat Technol* **202**(19): 4868–4874 (2008)
- [9] Wei A G, Tang Y, Tong T, Wan F, Yang S S, Wang K M. Effect of WC on microstructure and wear resistance of Fe-based coating fabricated by laser cladding. *Coatings* **12**(8): 1209 (2022)
- [10] Souza M E P, Ariza E, Ballester M, Rocha L A, Freire C M A. Comparative behaviour in terms of wear and corrosion resistance of galvanized and zinc-iron coated steels. *Matéria (Rio J)* **12**(4): 618–623 (2007)
- [11] Pinger T, Brand M, Grothe S, Marginean G. Abrasive wear behavior of batch hot-dip galvanized coatings. *Materials* **17**(7): 1547 (2024)
- [12] Liu H Y, Liu J N, Fu J, Zhao J, Sun Z H, Huang W C, Su Y H. Study on environmental corrosion performance of hot dip galvanizing coating. *J Phys Conf Ser* **2390**(1): 012007 (2022)
- [13] Hussain A K, Seetharamaiah N, Pichumani M, Chakra C S. Research progress in organic zinc rich primer coatings for cathodic protection of metals—A comprehensive review. *Prog Org Coat* **153**: 106040 (2021)
- [14] Gerengi H, Solomon M M, Marashi M, Kohen B B. A comparative analysis of the corrosion characteristics of electro-galvanized steel coated with epoxy zinc-free and zinc-rich coatings in 5% NaCl. *J Adhes Sci Technol* **37**(20): 2795–2806 (2023)
- [15] Lin B, Zhang L, Cai M, Lu J F, Yin J N, Huang Y, Zhang Y H, Fan X Q, Zhu M H. Synergistic anti-wear performance of zinc-rich epoxy coating on shot peening strengthened Q345 steel. *Surf Topogr: Metrol Prop* **11**(4): 045006 (2023)
- [16] Özkan D, Erarslan Y, Kıncaç C, Gürlü O, Yağcı M B. Wear and corrosion resistance enhancement of chromium surfaces through graphene oxide coating. *Surf Coat Technol* **391**: 125595 (2020)
- [17] Wu T, Chen Y X, Lin B, Yu L T, Gui W Y, Li J H, Wu Y, Zeng D W. Effects of WC on the microstructure, wear and corrosion resistance of laser-deposited CoCrFeNi high entropy alloy coatings. *Coatings* **12**(7): 985 (2022)
- [18] Velten K, Reinicke R, Friedrich K. Wear volume prediction with artificial neural networks. *Tribol Int* **33**(10): 731–736 (2000)
- [19] Hsu S M, Shen M. Wear prediction of ceramics. *Wear* **256**(9–10): 867–878 (2004)
- [20] Abdelgaied A, Liu F, Brockett C, Jennings L, Fisher J, Jin Z M. Computational wear prediction of artificial knee joints based on a new wear law and formulation. *J Biomech* **44**(6): 1108–1116 (2011)
- [21] Liu B B, Bruni S, Lewis R. Numerical calculation of wear in rolling contact based on the Archard equation: Effect of contact parameters and consideration of uncertainties. *Wear* **490**: 204188 (2022)
- [22] Zhang Z Y, Song Y X, Xu C G, Guo D M. A novel model for undeformed nanometer chips of soft-brittle HgCdTe films induced by ultrafine diamond grits. *Scripta Mater* **67**(2): 197–200 (2012)
- [23] Zhang Z Y, Wang B, Kang R K, Zhang B, Guo D M. Changes in surface layer of silicon wafers from diamond scratching. *CIRP Ann* **64**(1): 349–352 (2015)
- [24] Zhang Z Y, Cui J F, Wang B, Wang Z G, Kang R K, Guo D M. A novel approach of mechanical chemical grinding. *J Alloys Compd* **726**: 514–524 (2017)
- [25] Cao W, Han Z, Chen Z Q, Jin Z L, Wu J J, Qu J X, Wang D. The influence of wear volume on surface quality in grinding process based on wear prediction model. *The International Journal of Advanced Manufacturing Technology* **121**(9): 5793–5809 (2022)
- [26] Wang S C, Yang X C, Li X M, Chai C, Wang G, Wang X H. Simulation and experimental study on wear of U-shaped rings of power connection fittings under strong wind environment. *Materials* **14**(4): 735 (2021)
- [27] Nepal M, Vozár M. Assessment of cutting tool wear using a numerical FEM simulation model. *J Phys Conf Ser* **2712**(1): 012021 (2024)
- [28] Long H Y, Hao W, Ma R C, Gui Y L, Song C Y, Qin T Y, Zhang X F. Effect of temperature and load on tribological behavior in laser-cladded FeCrSiNiCoC coatings. *Materials* **16**(8): 3263 (2023)
- [29] Qi T, Zhao Y Z, A-akhali A, Cai J B, He F Q, Tang Z Q. Wear performance of Ti/Al composite coating based on magnetron sputtering. *J Phys Conf Ser* **1653**(1): 012044 (2020)
- [30] Shan L, Wang Y X, Zhang Y R, Zhang Q, Xue Q J. Tribocorrosion behaviors of PVD CrN coated stainless steel in seawater. *Wear* **362**: 97–104 (2016)
- [31] Lee H B, Lin C S, Wu D S, Lee C Y. Wear and corrosion investigation on the electrodeposited Ni-P coating. *Tribol T* **54**(4): 497–504 (2011)
- [32] Cai Z B, Chen Z Q, Sun Y, Jin J Y, Peng J F, Zhu M H. Development of a novel cycling impact-sliding wear rig to investigate the complex friction motion. *Friction* **7**(1): 32–43 (2019)
- [33] Xue Z Y, Hao X Y, Huang Y, Gu L Y, Ren Y, Zheng R P. Wear resistance and wear mechanism of a hot dip aluminized steel in sliding wear test. *Surf Rev Lett* **23**(2): 1550098 (2016)
- [34] Buciumeanu M, Araujo A, Carvalho O, Miranda G, Souza J C M, Silva F S, Henriques B. Study of the tribocorrosion behaviour of Ti₆Al₄V–HA biocomposites. *Tribol Int* **107**: 77–84 (2017)
- [35] Fedrizzi L, Valentinelli L, Rossi S, Segna S. Tribocorrosion behaviour of HVOF cermet coatings. *Corros Sci* **49**(7): 2781–2799 (2007)
- [36] Azzi M, Paquette M, Szpunar J A, Klemberg-Sapieha J E, Martinu L. Tribocorrosion behaviour of DLC-coated 316L stainless steel. *Wear* **267**(5–8): 860–866 (2009)
- [37] Sun Y, Rana V. Tribocorrosion behaviour of AISI 304 stainless steel in 0.5 M NaCl solution. *Mater Chem Phys* **129**(1–2): 138–147 (2011)
- [38] Chen K, Pan H B, Wu M Y, Wang X F, Li D Y. Wear-resistant Fe₆AlCoCrNi medium-entropy alloy coating made by laser cladding. *Metals-Basel* **12**(10): 1686 (2022)



- [39] Mahade S, Awe S A, Björklund S, Lukáč F, Mušálek R, Joshi S. Sliding wear behavior of a sustainable Fe-based coating and its damage mechanisms. *Wear* **500**: 204375 (2022)
- [40] Khun N W, Tan A W Y, Sun W, Liu E. Wear and corrosion resistance of thick Ti-6Al-4V coating deposited on Ti-6Al-4V substrate via high-pressure cold spray. *J Therm Spray Techn* **26**(6): 1393–1407 (2017)
- [41] Juhl M, Hauschild M Z, Dam-Johansen K. Sustainability of corrosion protection for offshore wind turbine towers. *Prog Org Coat* **186**: 107998 (2024)
- [42] Chen B B, Dong Z, Li J Y, Zhang M J, Zhang K. ZnO nanowires-decorated h-BN hybrid for enhancing the tribological properties of epoxy resin. *Prog Org Coat* **161**: 106493 (2021)
- [43] Hegadekatte V, Huber N, Kraft O. Finite element based simulation of dry sliding wear. *Model Simul Mater Sc* **13**(1): 57–75 (2005)
- [44] Yu L. Conic volume ratio of the packing cone associate to a convex body. *Geometriae Dedicata* **160**(1): 219–228 (2012)
- [45] Aghababaei R, Zhao K. Micromechanics of material detachment during adhesive wear: A numerical assessment of Archard's wear model. *Wear* **476**: 203739 (2021)



Ke Ning received his Ph.D. degree in mechanical engineering from Taiyuan University of Science and Technology, China, in 2022. Then, he joined the Engineering Research Center Heavy Machinery Ministry, Taiyuan University of Science and Technology, China. His current position is an associate professor and his research areas cover surface and interface coating design and tribology.



Qi Wang received his B.S. degree in mechanical and electronic engineering from Shandong Jiaotong University, China, in 2018. He is studying for a M.S. degree in Taiyuan University of Science and Technology, China. His research interests focus on surface modification and tribology.



Jianmei Wang received his Ph.D. degree in mechanical and electronic engineering from Taiyuan University of Technology, China, in 2009. Her current position is a professor and a Ph.D. supervisor at Engineering Research Center Heavy Machinery Ministry, Taiyuan University of Science and Technology, China. Her research areas cover tribology and surface interface technology of high-end equipment.



Wengang Ning received his B.S. degree in mechanical engineering from Shenyang University of Technology, China, in 2009. His current position is a senior engineer at Taiyuan Heavy Industry Co., Ltd., China. His research areas cover the development of large wind turbine generator sets.